Cell Stem Cell
Article

Neonatal Chimerization with Human Glial Progenitor Cells Can Both Remyelinate and Rescue the Otherwise Lethally Hypomyelinated Shiverer Mouse

Martha S. Windrem,[1] Steven J. Schanz,[1] Min Guo,[1] Guo-Feng Tian,[2] Vaughn Washco,[1] Nancy Stanwood,[3] Matthew Rasband,[4] Neeta S. Roy,[5] Maiken Nedergaard,[2] Leif A. Havton,[6] Su Wang,[1] and Steven A. Goldman[1,2,*]
[1]Department of Neurology
[2]Department of Neurosurgery
[3]Department of Obstetrics and Gynecology
University of Rochester Medical Center, Rochester, NY 14642, USA
[4]Department of Neurobiology, Baylor University College of Medicine, Houston, TX 77030, USA
[5]Department of Neurology and Neuroscience, Weill Medical College of Cornell University, New York, NY 10065, USA
[6]Department of Neurology, UCLA Medical Center, Los Angeles, CA 90095, USA
*Correspondence: steven_goldman@urmc.rochester.edu
DOI 10.1016/j.stem.2008.03.020

SUMMARY

Congenitally hypomyelinated shiverer mice fail to generate compact myelin and die by 18–21 weeks of age. Using multifocal anterior and posterior fossa delivery of sorted fetal human glial progenitor cells into neonatal shiverer × rag2$^{-/-}$ mice, we achieved whole neuraxis myelination of the engrafted hosts, which in a significant fraction of cases rescued this otherwise lethal phenotype. The transplanted mice exhibited greatly prolonged survival with progressive resolution of their neurological deficits. Substantial myelination in multiple regions was accompanied by the acquisition of normal nodes of Ranvier and transcallosal conduction velocities, ultrastructurally normal and complete myelination of most axons, and a restoration of a substantially normal neurological phenotype. Notably, the resultant mice were cerebral chimeras, with murine gray matter but a predominantly human white matter glial composition. These data demonstrate that the neonatal transplantation of human glial progenitor cells can effectively treat disorders of congenital and perinatal hypomyelination.

INTRODUCTION

Glial progenitor cells and the neural stem cells from which they derive may be isolated and transplanted into myelin-deficient hosts, as a means of introducing new oligodendrocytes able to myelinate host axons (Archer et al., 1997; Eftekharpour et al., 2007; Learish et al., 1999; Mitome et al., 2001; Yandava et al., 1999). We have previously noted that enriched preparations of human glial progenitor cells, when engrafted into the neonatal shiverer mouse—a mutant that lacks full-length myelin basic protein (Popko et al., 1987; Readhead et al., 1987; Roach et al., 1985)—generate substantial myelin in these otherwise unmyelinated recipients (Windrem et al., 2004) However, the potential utility of this approach to the development of clinical remyelination strategies has been unclear, as previous studies have failed to note significant brainstem, cerebellar, or spinal engraftment from intracerebral grafts, and no effect on disease phenotype or survival has yet been reported in hypomyelinated mice as a consequence of progenitor cell transplantation (reviewed in Goldman, 2005; Keyoung and Goldman, 2007). Our initial study of the efficacy of isolated human glial progenitors revealed no overt effect of cell transplantation on either the condition or fate of the engrafted recipients; despite widespread forebrain myelination, the transplanted mice typically died between 18 and 21 weeks of age, just as did unengrafted shiverers.

In the present study, using a newly developed set of approaches to cell acquisition and transplantation, we attempted a far more extensive and higher-density cell engraftment than any previously noted. Our aim in doing so was to achieve sufficiently widespread central myelination so as to influence the phenotype and survival of the recipient animals. To avoid rejection as a complicating variable in these experiments, we crossed shiverers with *rag2* null immunodeficient mice (Shinkai et al., 1992), and thereby generated an immunodeficient line of congenitally hypomyelinated mice in which to assess graft efficacy and effect. Using these double-homozygous rag2$^{-/-}$ × shiverer$^{shi/shi}$ mice, we established a multisite injection protocol, with concurrent bilateral hemispheric and cerebellar cell injections delivered at birth. This procedure resulted in widespread donor cell engraftment throughout the neuraxis, with infiltration of the forebrain, brainstem, and cerebellum, and ultimately the spinal cord and roots. The engrafted human glial progenitor cells exhibited robust, efficient, and functional myelination, with progressive ensheathment of host axons and restoration of normal nodes of Ranvier and attendant conduction velocities. This ultimately led to the high-efficiency myelination of the major intracerebral, ascending, and descending tracts, the cranial nerves and intracranial ganglia, and the spinal cord to the thoracolumbar level. Most notably, the implanted animals exhibited a substantial recovery of normal neurological phenotype, such that a fraction were frankly rescued by perinatal transplantation, surviving well

over a year until sacrificed for histology, which revealed a remyelinated—and essentially humanized—central white matter. The neurological recovery and sustained survival of these transplanted mice was in sharp contrast to the fate of their untreated controls, which uniformly died by 5 months of age. To our knowledge, these data represent the first outright rescue of a congenital hypomyelinating disorder by means of a stem or progenitor cell transplantation and indicate that neonatal glial progenitor cell transplantation may prove an effective means of treating disorders of hereditary and perinatal hypomyelination.

RESULTS

Engrafted Shiverer Mice Exhibited Substantially Prolonged Survival

Newborn double-homozygous shiverer (shi/shi) × rag2$^{-/-}$ immunodeficient mice were implanted with either 300,000 human glial progenitor cells (GPCs; n = 26), with PBS vehicle control (n = 29), or with nothing (n = 59). Cells were delivered at five sites, including the anterior and posterior corpus callosa bilaterally, and the presumptive cerebellar peduncle as a single midline injection; PBS controls received equal volume injections at each site, while the no-injection controls were not injected. The mice were then returned to their mothers and allowed to develop normally, with weaning at 21 days and small-group housing thereafter. All mice were observed to undergo progressive neurological deterioration, typically first manifest by progressive truncal instability, worse upon ambulation, followed with marked hindlimb weakness by 14–16 weeks of age, and seizures beginning at 4–6 weeks but rapidly increasing in frequency by 18–19 weeks. Thus, by 18 weeks, all mice exhibited markedly impaired forward ambulation and frequent episodes of sustained seizures. Over a range of 130–150 days postnatally, all of the 29 PBS treated and 59 untreated control shiverer mice died, with median and mean (±SEM) survivals of 135.0 ± 1.4 and 132.4 ± 2.1 days, respectively.

In sharp contrast, of the 26 implanted mice, 20 died during this period, but 6 (23.1%) survived. Whereas the average survival of the untreated controls approximated 130 days, and none of the 88 total control mice survived to 150 days, these 6 implanted mice survived over 160 days, and 4 appeared to have been frankly rescued, surviving over a year before being sacrificed for analysis. Remarkably, these mice exhibited overtly improved neurological function, with decreased seizure incidence and improved mobility and self-care. Transplanted mice surviving beyond 190 days exhibited apparent treatment-dependent cure, with sustained survival over a year, accompanied by a virtually complete recovery of normal neurological phenotype. As a result, the engrafted mice as a group exhibited significantly prolonged survival: Kaplan-Meier analysis (Hosmer and Lemeshow, 1999) confirmed that the treatment-associated improvement in survival was statistically significant, and profoundly so ($p = 0.0003$; hazard ratio = 0.4718 (95% CI = 0.30–0.70) (Figure 1A).

Transplantation Was Associated with Neurological Improvement and Diminished Seizures

The rescued mice exhibited substantial resolution of their neurological deficits. Shiverer mice typically exhibit truncal instability and marked intention tremor, evident within weeks of birth, which becomes complicated by a progressive hindlimb weakness, and multimodal sensory and perceptual deficits that include blindness, such that by 18–19 weeks of age they are severely impaired (see Movie S1 available online). In addition, they manifest a progressively worsening seizure disorder (Movie S2), often succumbing to status epilepticus. Given the substantially longer survivals noted in a fraction of the transplanted shiverers, we asked what the behavioral concomitants were to transplantation, as a function of time after cell delivery. We were especially interested in any discernible differences in the behavior or neurological status of shiverer mice that were rescued by neonatal GPC transplant, relative to transplanted littermates that nonetheless died. We noted that all of the shiverers, both transplanted and controls, deteriorated identically over the first several months after birth and transplantation. Indeed, up to 130 days, the point at which mice typically began to die in number, little difference was observed in the behaviors of transplanted relative to untransplanted shiverer mice. However, those mice that survived the period spanning 130–150 days postnatally exhibited noticeable improvement in their neurological exams thereafter, frankly manifest by 7–8 months of age as diminished frequency of seizures and improved ambulation, with more forward motion and less retropulsion or freezing. Over the several months thereafter, the transplanted mice incrementally improved, regaining normal fluidity in ambulation and voluntary explorative behavior, and less truncal intention tremor. All five mice surviving to at least 35 weeks of age were substantially normal by that point and thereafter in terms of their grossly assessable neurological function, save for a coarse axial intention tremor, manifesting as a wobble on forward ambulation (Movie S3).

Because the death of most mice at 130–150 days of age was coincident with the period of sharply increasing seizure activity, we next assessed the frequency and duration of spontaneous seizures in untreated and transplanted shi/shi × rag2 nulls, as a function of age. We paid special attention to the incidence of seizures in transplanted mice that were rescued by transplant, compared with their treated counterparts that nonetheless succumbed. We found that the first seizures of shiverer mice—typically characterized by absence-like episodes of tonic akinesia, followed by a rapid evolution to brief tonic-clonic events—appeared by 35–42 days of age (Figure 1B). At approximately 120 days, the incidence of seizures was noted to substantially increase in treated and untreated animals alike. Over the period spanning 120–140 days, the seizure incidence of each group increased, yielding frequent seizures every hour (see Figure S1 for a representative EEG recording); these ictal events progressed to sustained periods of status epilepticus, often associated with death. However, in those animals that survived this period to enjoy long-term survival, seizure incidence fell dramatically, such that no seizure activity whatsoever was observed at 12 months ($p < 0.0001$ by one-way ANOVA, separately comparing 12-month transplanted animal seizure incidence to that of 4-month transplanted and control shiverers). Thus, perinatal GPC transplantation was associated with markedly diminished seizure activity in those shi/shi × rag2 null mice that were rescued by perinatal transplantation, such that by a year, none manifested any residual spontaneous seizure activity, while otherwise exhibiting virtually complete neurological recovery.

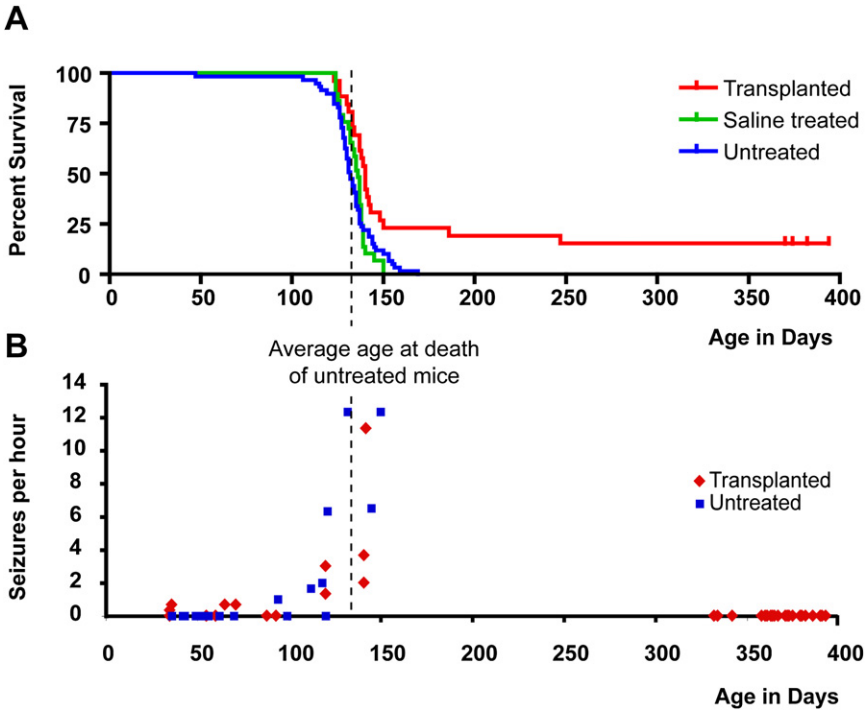

Figure 1. Engrafted Shiverer Mice Exhibited Substantially Prolonged Survival

(A) Shiverer/rag2$^{-/-}$ mice, either engrafted with human glial progenitor cells (GPCs) at birth (n = 26, red), injected with saline (n = 29, green), or untreated (n = 59, blue) were maintained in small-group housing and monitored daily until death. The Kaplan-Meier survival graph, plotting the percentage of each group alive as a function of age in weeks, shows that most mice die between 18 and 21 weeks. However, a fraction of engrafted mice (n = 6, or 23.1%) lived substantially longer than any control mouse; four survived more than 1 year, at which point the experiment was terminated.

(B) Shiverer mice uniformly manifested a seizure disorder that was typically apparent by 10 weeks of age, and then worsened between 16 and 18 weeks. When seizure frequency was scored by video with blinded post hoc assessment, transplanted and control shiverers both were noted to seize frequently during weeks 18–21, corresponding to the time span during which most mice died. However, the seizure incidence among the transplanted shiverers fell thereafter, such that by 47 weeks of age, all surviving mice were seizure free.

Besides spontaneous seizures, we noted that shiverers exhibited stimulus-evoked seizure activity that increased in both frequency and duration as a function of age. To quantify this pathological response to handling, we established a brief screening test by which mice were briefly and abruptly suspended by the tail, and their behavioral responses observed. We found that such tail suspension was sufficient to induce seizures in a large proportion of shiverer mice, whether treated or not, by 3 months of age. The induction of seizure activity within 30 s of tail suspension was thus chosen as a metric by which to assess the effect of cell transplant on seizure incidence and duration. We observed that among the transplanted shiverers, the percentage of individual tail suspension challenges resulting in clinically overt seizures rose to 75% ± 2.4% by 3–4 months. Among the transplanted mice that survived at least 5 months, 47% ± 2.8% of tail suspension challenges resulted in seizures. In contrast, by 8 months, none of the four surviving mice could be induced to seize by tail suspension. Linear regression of the percentage of mice induced to seize, plotted against their age in days, revealed a best fit of $y = -0.324x + 116.7$. Regression analysis confirmed that the negative correlation between seizure incidence and age ($r = 0.826$; $r^2 = 0.68$) was significant ($p < 0.0001$; $F = 53.68$ [1, 25 df]) (see Figure S2).

Although these data do not yet allow us to causally attribute the sustained survival of these transplanted shiverers to the diminution of their seizure activity, the increased incidence of spontaneous and stimulus-evoked seizures coincident with the period during which most shiverers die, coupled with the diminished seizure incidence of those transplanted survivors that go on to survive (cf. Figures 1B and 1A), suggests that improved seizure control contributes to the sustained viability of the long-surviving transplant recipients.

Perinatal Grafts of Human Glial Progenitors Yield Widespread and Dense Host Myelination

To assess the terminal distribution of donor cells and robustness of myelination in the transplanted animals, and to compare the extent of donor cell dispersal and myelination between short- and long-term survivors, the latter were ultimately sacrificed at 13 months of age, after assessment of their transcallosal conduction velocities and seizure frequency. The brains and spinal cords of these mice were then analyzed in terms of donor cell distribution and density; myelin production and the proportion of myelinated axons; nodal architecture and reconstitution; and ultrastructural metrics, including myelinated axons and myelin G ratios. Each of these metrics was then compared to those obtained from transplanted mice that had died earlier, as well as to unimplanted shiverer controls and wild-type, normally myelinated, rag2 null mice.

These histological data supported the compelling nature of the survival data. Human donor-cell engraftment was extraordinarily extensive, with essentially whole neuraxis penetration and colonization by the human GPCs (Figure 2A). High donor-cell densities were observed throughout the forebrain, cerebellum, brainstem, and cervical spinal cord, diminishing only at the level of the thoracolumbar cord, yet increasing again in the sacral cord and conus medullaris. The pattern of myelination, as indicated by MBP expression, reflected this widespread engraftment, with equally widespread and dense myelination (Figures 2B–2F), including not only all major central white matter tracts but also structures as distant and diverse as the cranial ganglia, optic chiasm, and conus medullaris (e.g., Figure 2G). These long-term survivors, whose neurological exams had largely normalized by 9 months of age, exhibited essentially complete myelination of the brain, brainstem, and cerebellum, with substantial myelination of the optic nerves (Figure 2B), spinal cord (Figure 2E), and

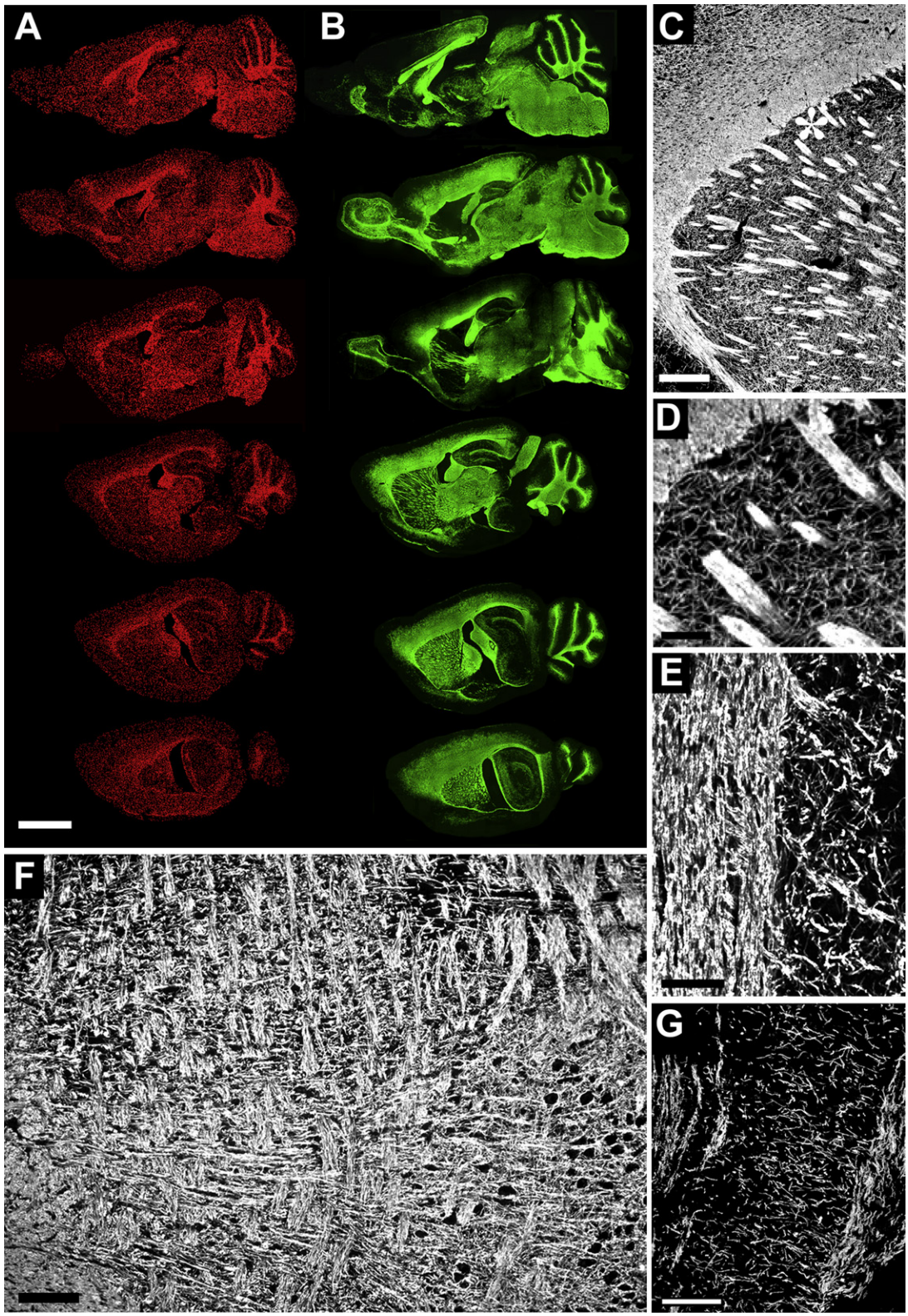

Figure 2. Perinatal Grafts of Human Glial Progenitors Yield Widespread and Dense Host Myelination

(A and B) Serial sagittal images of an engrafted shi/shi × rag2$^{-/-}$ brain, sacrificed at 1 year of age. Each image in (A) and (B) represents a montage of 50–100 images at 10×. Each series begins 750 μm lateral to the midline and continues at 600 μm intervals. (A) Human donor cells, immunolabeled in 14 μm cryosections using an antihuman nuclear antibody (hN; red). (B) Alexa 488-labeled myelin basic protein (MBP; green) in sections adjacent or nearly so to their

spinal roots (Figure 2G), as well as of the cranial roots and ganglia (Figures 3A–3C). In regards to the latter, the cessation of donor GPC migration at the border of CNS and PNS was striking, such that donor-derived myelination occurred up to, but not beyond, the transition points demarcating central ganglia and roots from peripheral nerve (Figures 3A–3E). The resultant densities and patterns of donor cell dispersal resulted in the virtually complete chimerization of the murine hosts' central nervous systems, which thereby acquired a largely humanized white matter. Three-dimensional reconstructions confirmed that both the pattern and density of donor-derived myelination in the brains of transplanted shiverers approximated that of wild-type, normal mice.

Xenografted Shiverer Brains Exhibit Restored Nodes of Ranvier

We next asked if donor cell-derived myelination of shiverer axons was accompanied by the acquisition of normal nodes of Ranvier and paranodal structure (Figures 4A–4D). Using high-resolution confocal imaging of the corpus callosa, cervical spinal cords, and optic nerves of implanted shiverers killed at 35 or 52 weeks of age, we assessed the distribution pattern of the paranodal and juxtaparanodal proteins Caspr and the $K_V1.2$ voltage-gated potassium channel, respectively—the contiguous interaction of which characterizes the normal node of Ranvier (Rasband and Trimmer, 2001; Schafer and Rasband, 2006). These potassium channels are assembled at—and functionally define—the juxtaparanodes in myelinated axons, but they are broadly and nonspecifically expressed in unmyelinated fibers (Rasband and Trimmer, 2001). In addition, we determined the axonal expression and compartmentalization of $Na_V1.6$ fast sodium channels, which are typically sequestered at nodes of Ranvier in intact myelinated axons but dispersed broadly along unmyelinated or dysmyelinated fibers. Similarly, we immunostained for βIV spectrin, which couples to ankyrin to organize fast sodium channels at the node of Ranvier, and hence typically coincides with nodal Nav1.6 expression (Schafer and Rasband, 2006; Sherman and Brophy, 2005; Yang et al., 2007).

Using these complementary nodal markers, we identified an essentially normal organization of the nodes of Ranvier in transplanted mice, which was indistinguishable from that of wild-type mice. Caspr and $K_V1.2$ were expressed in organized paranodal and juxtaparanodal apposition, with an expression pattern that contrasted sharply with the grossly uncoordinated pattern of diffuse Caspr and $K_V1.2$ immunolabeling that was evident in the untransplanted controls (Figures 4A–4D). Similarly, both $Na_V1.6$ (Figures 4A″–4D′) and βIV spectrin (Figures 4A″–4D″) clearly identified nodes of Ranvier in the transplanted shi/shi mice, flanked by Caspr defining the paranodes; their untransplanted controls showed no such sequestration of either $Na_V1.6$ or βIV spectrin expression. Together, these observations suggest that despite interspecies chimerization, the glioaxonal interactions of human GPC-derived oligodendrocytes with host mouse axons were functionally appropriate. More broadly, they indicate that GPC-derived oligodendrocytes are able to communicate effectively with host axons, organizing structurally appropriate nodes of Ranvier while sequestering fast sodium channels within the nodes, and thereby myelinating their axonal substrates effectively and appropriately.

Transcallosal Conduction Velocities Are Restored in Xenografted Shiverer Brains

In light of the apparent histological reconstitution of normal myelin, we next asked if donor OPC-derived myelin was sufficient in extent and functional competence to restore the conduction speed of newly myelinated central axons. To this end, we assessed the conduction velocity across the corpus callosum in a sample of four long-surviving transplanted shiverer mice 12–13 months after neonatal xenograft. The transcallosal nerve conduction velocities were determined by recording response amplitudes and times from depth electrodes placed bilaterally in the corpus callosa of each of these mice, after contralateral stimulation at symmetric sites during open craniotomy. Equal numbers of age-matched wild-type (congenic C3H) mice and rag2 null controls were assessed identically, as was a necessarily younger (4 months old) sample of untransplanted shiverer × rag2 null mice. As this was a terminal procedure, these animals—all of which had exhibited not only sustained survival but also a substantial restoration of normal neurological function—were sacrificed after measurement of their transcallosal conduction velocities, thus ending the survival study in which they were subjects.

We found that though control Fvb wild-type (n = 3) and rag2 null C3H mice (n = 4) exhibited conduction velocities of 0.324 ± 0.01 and 0.328 ± 0.03 m/sec respectively, the shiverer × rag2 mice (n = 4), also on the C3H background, exhibited substantially slower conduction, at 0.260 ± 0.02 m/sec (Figure 4E). In contrast, transplanted shiverer × $rag2^{-/-}$ mice, tested just prior to sacrifice 12–13 months posttransplant (n = 3), had an average conduction velocity of 0.330 ± 0.01 m/sec. Repeated-measures ANOVA with post hoc Boneferroni t tests revealed a significant treatment effect ($F = 35.15$ [3, 9 df]), such that callosal conduction by the transplanted mice was significantly faster than untransplanted shiverer × $rag2^{-/-}$ mice ($p < 0.001$), and indistinguishable from that of normally myelinated Fvb wild-type and rag2 null mice. The more rapid transcallosal conduction exhibited by the transplanted mice was sustained across stimulus intensities, and thus appeared to represent improved conduction across a wide spectrum of fiber diameters (Figure 4F). Thus, neonatal transplantation of human OPCs yielded sufficient myelin, in terms of both density and physiological competence, to restore normal interhemispheric conduction velocity to a major central tract, the corpus callosum.

matched sections in (A). All major white matter tracts, including those of the corpus callosum, capsules, striatum, fimbria, cerebellum, and brainstem heavily express MBP.

(C–G) Black-and-white images of MBP-immunoreactive fibers in a number of sites reveal high-efficiency axonal myelination; all images of transplanted shi/shi × $rag2^{-/-}$ mice at >1 year posttransplant. (C) The rostral striatum, corpus callosum, and neocortical layers 5 and 6 are shown in sagittal section. (D) Higher magnification of (C) shows the MBP-defined myelination of individual fibers within the striatum, as well as the larger bundles of corticostriatal and striopallidal fibers. (E) Donor-myelinated MBP^+ fibers in a longitudinal section of the cervical spinal cord; dorsal column to the left, central gray to the right. (F) Interwoven donor-myelinated fibers of the brainstem, in the pontine base. (G) Donor-derived MBP in the conus medullaris; exiting myelinated roots of the cauda equina to the left. Scale bars: 2.5 mm in (A) and (B), 200 μm in (C), 40 μm in (D), 50 μm in (E), 60 μm in (F), and 125 μm in (G).

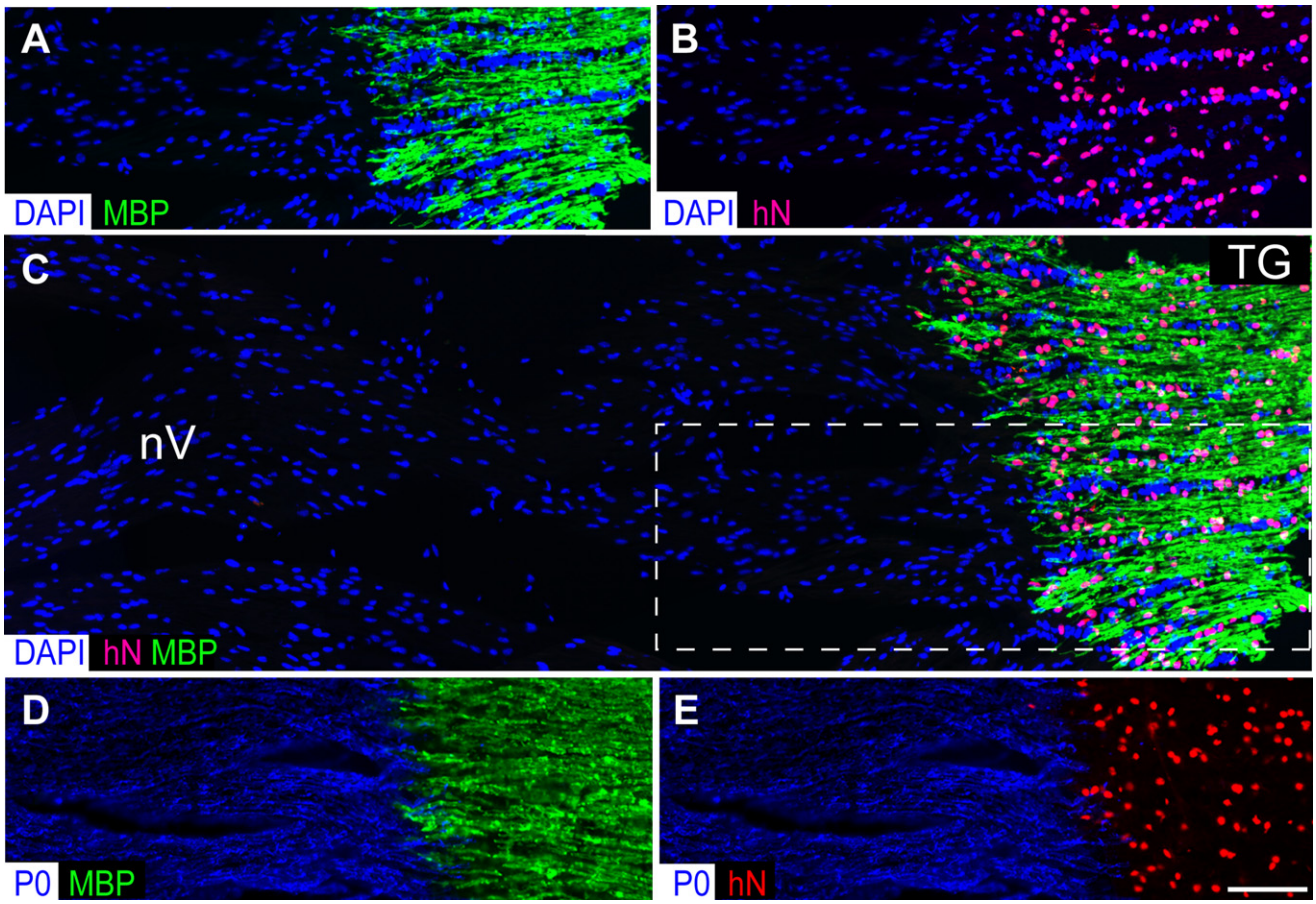

Figure 3. Transplanted GPCs Invade the Cranial and Spinal Roots but Obey the CNS-PNS Border

Transplanted mice exhibited robust myelination throughout the entire CNS neuraxis by 9 months of age, that included not only the brain, brainstem, cerebellum, and spinal cord, but also the cranial nerves, ganglia, and both cranial and spinal roots (see Figures 2 and 4). Of note, the invasion of human glial progenitor cells, all derived from the fetal forebrain, was sharply delimited to the CNS, with no invasion whatsoever of the peripheral nerves beyond the root takeoffs.

(A and B) Dense concentration of human donor cells (antihuman nuclear antigen, red) in the trigeminal ganglion (TG) and the concurrent prohibition of donor cell infiltration into the trigeminal nerve (nV), a peripheral nerve. Accordingly, donor-derived myelin (MBP, green) was limited to the ganglion and trigeminal nerve takeoff, and did not extend into nV proper.

(C) A wider field color composite of (A) and (B), which correspond to the boxed area of (C), further demonstrating that the transplanted GPCs strictly respect the CNS-PNS border. In contrast, (D) and (E) show an adjacent section stained for the peripheral myelin protein P0 (blue) and for either human nuclear antigen (red) or central myelin basic protein (green). The human cells are seen to have stopped at the P0 protein-defined threshold to the PNS. Scale bar: 50 μm.

Myelination and Axonal Ensheathment Were Progressive over Time

We had previously established that the dispersal of donor cells following neonatal implantation of human GPCs was relatively rapid, with the terminal distributions of engrafted progenitors occurring within 4–8 weeks of neonatal administration, and myelination proceeding over the several months thereafter (Windrem et al., 2004). In the present study, given the extended survival of mice transplanted both in brain and brainstem, we were able to assess the later progression of myelination in the graft recipients. We asked whether myelination continued to progress even after extended survival had been achieved. To that end, we examined the brains of transplanted shiverers at 18–20 (n = 10), 27 (n = 1), 35 (n = 1), and 52–56 (n = 4) weeks of age, and assessed the distribution pattern and densities of human donor cells, as well as of donor-derived myelin, in these recipient brains. (The 20-week-olds had died natural deaths despite their extensive donor cell engraftment, whereas the 52- to 56-week-olds were long survivors, which had been killed to allow histological analysis. The deaths of the 27- and 35-week-old mice (natural and accidental deaths, respectively) provided informative, if singular, intermediate time points.

We found that though cerebral and cerebellar myelination, as followed by MBP expression, were substantial and geographically widespread at 20 weeks, both the density and distribution of MBP expression in the brainstem and cervical spinal cord were more extensive at 35 weeks than 20, and much more so at 52–56 weeks (Figures 5A–5C and 5D–5F). In particular, the 52- to 56-week-old transplanted mice exhibited essentially complete myelination of the brainstem (Figure 5C; also Figure 2B), whereas the 20-week-olds still exhibited a number of regions of relative hypomyelination relative to wild-type controls (Figure 5A). The areas of relatively delayed myelination included the ventral long tracts of the brainstem, as well as the brainstem

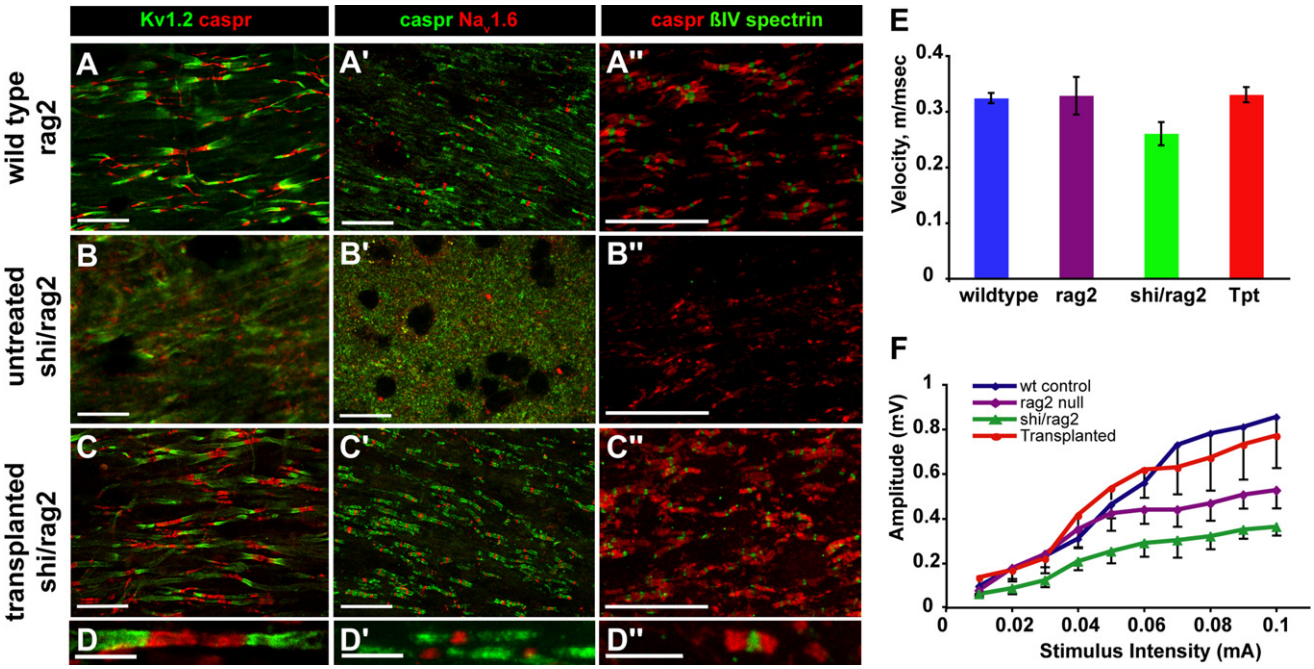

Figure 4. Engrafted shi/shi Brains Exhibit Restored Nodes of Ranvier and Callosal Conduction Velocities

The expression patterns of several antigens characteristic of nodes of Ranvier, including nodal ($Na_V1.6$, βIV-spectrin), paranodal (Caspr) and juxtaparanodal ($K_V1.2$) proteins, were investigated in the spinal cord ([A–D] and [A′–D′]) and optic nerves (A″–D″) of normally myelinated wild-type ($rag2^{-/-}$) mice (A–A″), and compared to the corresponding expression patterns in the optic nerves of both untreated (B–B″), and transplanted ([C–C″] and [D–D″]) shiverer × $rag2^{-/-}$ mice. The nodal architecture of the transplanted shiverers was indistinguishable from that of wild-type controls for every antigen tested; both exhibited the sodium channel and spectrin clustering, flanked by the paranodal Caspr and juxtaparanodal Kv1.2, of mature nodes. The nodal integrity of the transplanted shiverers ([C–C″]and [D–D″]) contrasted sharply to the disorganized and indistinct antigen expression patterns of the untreated mice (B–B″), in which neither nodal channel clustering nor paranodal Caspr sequestration was noted. (E and F) Transcallosal responses were evoked by electrical stimulation in mice in vivo. (E) Ttranscallosal conduction velocities obtained from wild-type, $rag2^{-/-}$, shiverer × $rag2^{-/-}$, and transplanted shiverer × $rag2^{-/-}$ mice, all assessed between 12 and 13 months after neonatal transplant. (F) Relationship between stimulus intensity and signal amplitude in C3H wild-type mice, $rag2^{-/-}$ mice, shiverer × $rag2^{-/-}$ mice, and transplanted shiverer × $rag2^{-/-}$ mice, respectively.

tegmentum and intrinsic internuclear tracts, all of which were more extensively myelinated at 52 weeks of age than at earlier time points. By scoring the proportion of ensheathed host axons in confocal optical sections immunostained for MBP and neurofilament, we found that by 52 weeks, 78.0% ± 4.8% of axons in the cervical corticospinal tract at the cervicomedullary junction were myelinated (Figure 5H), a marginally smaller proportion than that observed in wild-types (93.9% ± 0.9%). By that time point, the proportion of myelinated axons in the corpus callosum of the transplanted animals was similarly indistinguishable from that of the wild-type controls; each exceeded 60% (Figure 5G). We next used transmission electron microscopy (TEM), concentrating on the longitudinal and largely parallel fibers of the cervical spinal cord, to validate the criteria by which we defined myelin-ensheathed axons in our confocal analysis. TEM of the cervical corticospinal tract of 12- to 13-month-old transplanted shiverers established that the majority of axons manifested ultrastructurally normal myelin, with both major dense lines and multilayer lamination (Figures 5I and 5K), thereby confirming that axons appearing ensheathed in confocal optical sections were indeed so. Furthermore, the major dense lines of the observed myelin indicated its necessarily donor cell origin, as shiverer oligodendrocytes do not make major dense lines; formation of the latter requires myelin basic protein, in which shiverers are genetically deficient (Readhead et al., 1990). In addition, the calculated G ratio, defined as the ratio of axonal diameter to total myelin-ensheathed fiber diameter, was significantly higher in the untreated shiverers than in either transplanted shiverers or wild-type rag2 nulls; the latter groups did not differ from one another (Figure 5L). This indicated that whereas untreated shiverers had little or no myelin ensheathment, their transplanted kindreds had myelin sheaths as thick, on average, as their normally myelinated wild-type × rag2 null controls.

The progressive myelination of transplanted shiverers did not appear to be a function of the rate or kinetics of donor cell dispersal, in that the topography of donor cells at 35 weeks did not differ substantially from that observed at 52 weeks. Nonetheless, the local densities of donor-derived cells did appear to rise over time; this rise was asymptotic (Figure 6A), which appeared to reflect the fall in mitotic competence of the donor cell pool following their initial expansion in the first half-year or so after transplantation (Figure 6B). These data suggest that long after human donor cells achieve their destinations, myelinogenesis and axonal ensheathment continue to progress slowly, ultimately achieving the myelination of the recipient neuraxis only after a protracted period of postnatal maturation; this may reflect the incremental engagement of local axons by single oligodendrocytes, as the latter mature and expand their individual domains of myelin

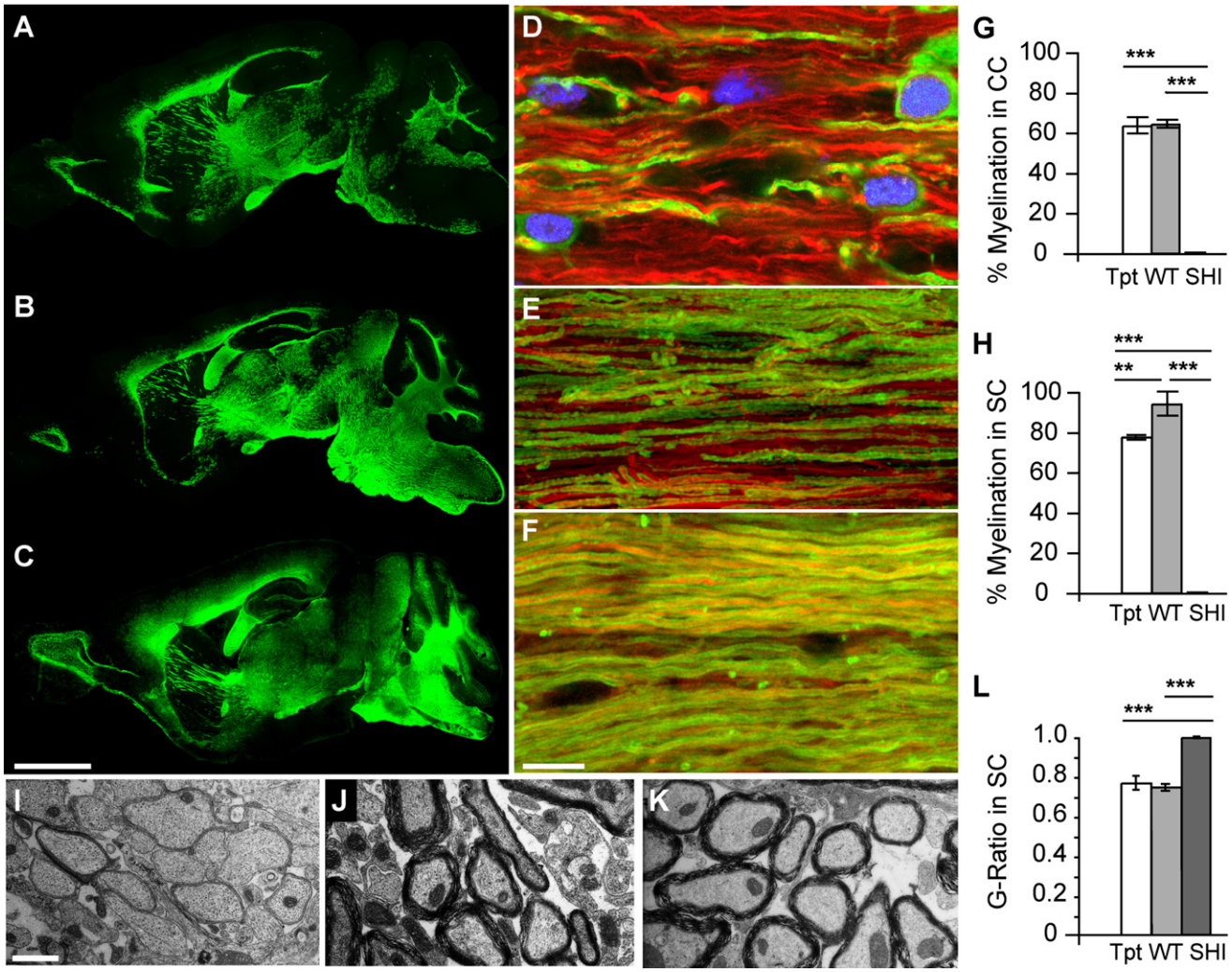

Figure 5. Myelination and Axonal Ensheathment Were Progressive over Time

(A–C) Sagittal sections of hGPC-implanted mice immunolabeled for MBP (green) at (A) 20 weeks; (B) 35 weeks; and (C) 52 weeks. (A) Major white-matter regions of the brain, including the corpus callosum, fimbria, optic tract, and both the cerebral and cerebellar peduncles, are already myelinated at 20 weeks. (B) At 35 weeks, the area of dense myelination has expanded into the midbrain and hindbrain. (C) By a year, myelin was well distributed, and myelination appeared complete, throughout the forebrain and hindbrain, including the lowers layers of neocortex, the colliculi, the pons and medulla, and the major corticopontine and corticospinal tracts.

(D–F) Corresponding confocal optical sections of transplanted shiverer mouse corpus callosum taken at (D) 20, (E) 35, and (F) 52 weeks, immunolabeled for neurofilament (red) and MBP (green), reveal the progressive increase in axonal ensheathment with time.

(G and H) The proportion of MBP-ensheathed axons, as determined by confocal analysis, in the (G) corpus callosa (CC) and (H) cervical corticospinal tracts of the spinal cord (SC) in 1-year-old transplanted shi/shi × rag2$^{-/-}$ mice compared to both untreated and wild-type rag2$^{-/-}$ controls. At both sites, most axons in the transplant recipients were ensheathed by MBP-defined myelin. In contrast, no ensheathment was noted in their untreated counterparts.

(I–K) Electron micrographs of spinal cord cross-sections in (I) untreated shi/shi × rag2$^{-/-}$ mice, (J) wild-type rag2$^{-/-}$ controls, and (K) 1-year-old transplanted shi/shi × rag2$^{-/-}$. (L) G ratios calculated in 1-year-old implanted shiverers, compared to their wild-type and untreated shiverer controls. The correlation between myelin sheath thickness and axonal diameter in implanted mice is indistinguishable from that of wt/rag2 null mice, whereas myelin sheaths are virtually undetectable in untreated shiverers. Scale bars: 2.5 mm in (A)–(C), 10 μm in (D)–(F), and 1 μm in (I)–(K).

ensheathment, adding axons to their ensheathed cohort one at a time over a period of many months.

Long-Term Survival Was Associated with Humanization of the Recipient White Matter

The selective expansion of the human glial population in the shiverer mouse white matter appears to be at least in part a product of the more sustained proliferation of the transplanted human GPCs (Figures 6B and 6D), which as derived from the late second-trimester fetal SVZ, would be expected to have continued actively dividing for at least another 9–12 months, assuming cell-autonomous regulation of expansion potential. Accordingly, when we plotted the number of all-human cells in the recipient mouse brains, as a function of time, we found that the initial dose of 300,000 cells per recipient had expanded to an average of 12 million human donor glia by 12–14 months in the long-term

survivors (Figure 6A). When the incidence of $Ki67^+$ cells was assessed in three sample regions—the corpus callosum, fimbria, and cerebellar white matter—the fraction of mitotic human donor cells was found to be much higher than that of the local host cells, both perinatally and for many months thereafter; only at a year after engraftment was the $Ki67^+$ fraction of human donor cells observed to fall below 2% (Figure 6B). Even then, the fraction of $Ki67^+$ human glia remained higher than the corresponding proportion of $Ki67^+$ mouse cells, in both the transplanted hosts and in the rag2 wild-type or shi/shi × $rag2^{-/-}$ mouse controls ($F = 12.42$ [3, 2 df] by two-way ANOVA permuting cell type and region; $p < 0.05$ for each comparison, by Boneferroni posthoc t tests) (Figure 6D). Ultimately, despite the preferential expansion of the human donor cell pool, its relative mitotic quiescence was achieved by a year after transplantation, according to the approximate time course by which normal human GPCs attenuate their expansion in situ. No evidence of heterotopic foci, anaplasia, or neoplastic transformation was noted in over 100 transplanted mice serially examined.

These data indicate that donor human GPCs exhibit more robust and sustained mitotic expansion than their host murine counterparts after transplantation and that, over time, this results in the relative humanization of the recipient white matter. Indeed, quantification of the human donor cell complement revealed that in four long-surviving transplanted mice sacrificed at 12–14 months, at least one-third of all cells in the corpus callosum, fimbria, and cerebellar white matter were of human origin (35.3% ± 11.8%, 42.9% ± 10.9%, and 40.8% ± 6.9%, respectively) (Figure 6C). In three of the four, over 40% of all cells in each of these white matter regions were human, and in the densest engraftment among these—that of a mouse sacrificed at 13 months—54.6% of all cells in its callosum were human. Because just under one- third of all cells in the shiverer white matter are nonglial (unpublished data)—these include microglia, endothelial cells, and pericytes—we estimate that at least 80% of all callosal glial cells in this "best case" mouse were of human origin by a year after engraftment; more broadly, over half of all callosal glia were human in each of the long-surviving recipients assessed.

DISCUSSION

In these experiments, we delivered highly enriched isolates of human glial progenitor cells into neonatal shiverer × rag2 null (shi/shi × $rag2^{-/-}$) immunodeficient and myelin-deficient mice, using a multifocal delivery strategy that achieved both widespread and dense donor cell engraftment throughout the recipient CNS. Our injection sites were chosen so as to permit contiguous infiltration of migrating donor cells into all major brain, brainstem, and spinal white-matter tracts, without hindrance from intervening gray matter structures that might delimit the migration and sustained multilineage competence of engrafted glial progenitor cells (Windrem et al., 2002). By this strategy, we achieved the complete, whole-neuraxis myelination of the engrafted hosts; in a fraction of these animals, this resulted in the effective rescue of this otherwise lethal phenotype. These mice exhibited essentially complete myelination of the brain, brainstem, and cerebellum, with substantial myelination of the optic nerves, cranial roots and ganglia, spinal cord, and spinal roots, that was associated with clinical rescue, as reflected by sustained survival and substantially restored functional competence—the latter as manifested electrophysiologically and behaviorally.

This transplant-associated reduction in morbidity and mortality was accompanied by the acquisition of normal nodes of Ranvier and paranodal structure, a restitution of transcallosal conduction velocity, ultrastructurally normal and complete myelination of the overwhelming majority of axons, and a restoration of a substantially normal neurological phenotype. These transplants were also attended by a virtually complete chimerization of the recipient central nervous system, such that the surviving recipients, and in particular the long-term survivors, developed a largely humanized white matter. Donor cell expansion occurred in an asymptotic fashion, such that chimerization evolved over the 8–9 months after transplantation, with progressive myelination reflecting ongoing axonal ensheathment as much as persistent cell expansion.

The progressive chimerization of the host white matter with admixed human donor cells was attended by a significant loss of host glial progenitor cells and oligodendroglia (data not shown). Whether the competitive strength of the human donor cells was the result of more effective axonal interactions by myelinogenic donor cells relative to nonmyelinogenic host progenitors, or rather reflected the selective mitotic expansion of the human donor cells in the postnatal murine environment, or even the selective geographic displacement of the host cells by their donor-derived counterparts, is unclear; it seems likely that each of these factors contributed to the marked competitive advantage of the human donor cells. Yet setting aside the nature of this donor-host competition, the degree of the resultant humanization was remarkable: by 13 months of age, over one-third of all cells, and the majority of the glial cells within the recipient callosa, fimbria, cerebellar white matter, and cervical spinal cords—indeed, in every region quantified—were human. Moreover, of the recipient axons in these regions, >60% were successfully ensheathed by donor oligodendrocytes; the nodal architecture of the resultant chimerized brains was thus established by human myelin-associated proteins. As a result, multifocal neonatal delivery of human glial progenitor cells to myelin-deficient immunodeficient mice—intended initially as a proof of principle of a promising therapeutic approach—has also provided us mice with largely humanized white matter (Figures 6E and 6F), in which the responses of human glial oligodendrocytes and astrocytes to injury and disease may now be observed in real time, in vivo. This may prove an invaluable experimental model going forward, apart from the value of somatic chimerization via progenitor cell allografts as a potential therapeutic approach in the dysmyelinating disorders.

Several reports have noted the potential utility of neural stem or progenitor cell grafts in alleviating pathology in congenital leukodystrophies associated with lysosomal storage disorders; these efforts have capitalized on the provision of wild-type enzyme by engrafted donor cells to the otherwise deficient host cells with which they structurally integrate (Lee et al., 2007; Pellegatta et al., 2006; Snyder et al., 1995). Yet no cell-based treatment of any congenital hypomyelination has ever proven sufficient to rescue the underlying phenotype. A number of previous studies demonstrated that transplants of fetal tissue (Lachapelle et al., 1983), tissue dissociates (Gumpel et al.,

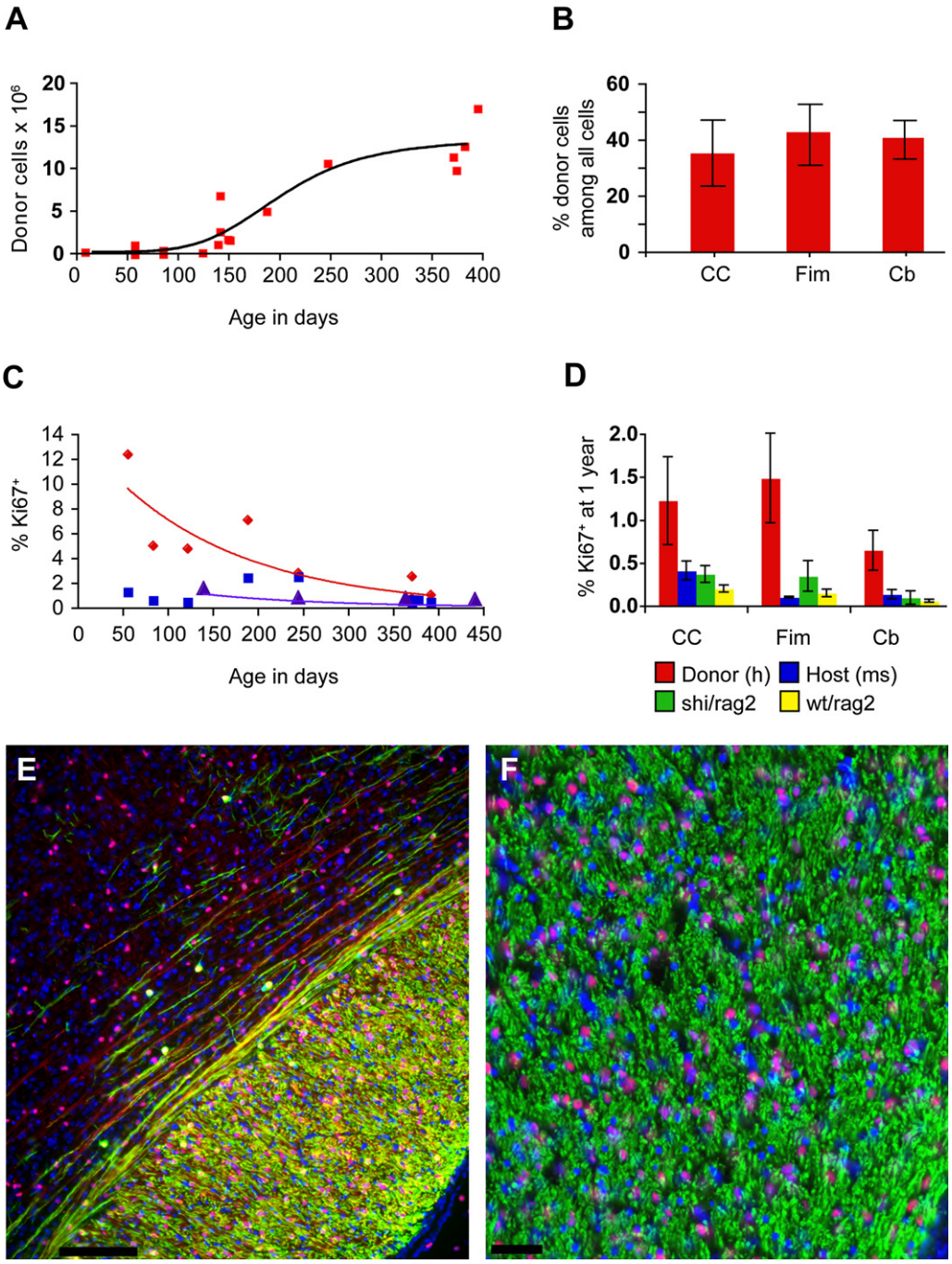

Figure 6. Long-Term Survival Was Associated with Humanization of the Recipient White Matter

(A) Perinatally transplanted human GPCs increase in number asymptotically over the course of a year. From an initial dose of 300,000 on postnatal day 1, the cells increase to an average of 12 million/brain by 1 year posttransplantation ($y = -9{,}898{,}000 + 733{,}632x + (-5709)^2$; $r^2 = 0.83$).

(B) By 1 year, donor cells comprised over 40% of all cells in the fimbria and cerebellar white matter, and over one-third in the corpus callosum. Because the total cell count includes host vascular cells and microglia, the human donor-derived cells appeared to comprise a net majority of all glial cells by that stage.

(C) Over the year after implantation, the rate of human GPC proliferation in white matter declined exponentially (red; $y = 14.013e^{-0.0475x}$; $r^2 = 0.79$). At 8 weeks, 12.35% of human GPCs in the mouse corpus callosum are Ki67$^+$, but by 1 year, an average of 1.22% are Ki67$^+$. From 5 to 12 months, the percentage of Ki67$^+$ mouse cells in the corpus callosum of untreated rag2 null mice also declines exponentially, but beginning at a lower rate (purple; $y = 2.9154e^{-0.0497x}$; $r^2 = 0.83$). The Ki67$^+$ percentages of endogenous mouse cells in the same sections of transplanted mice from which the hGPC percentages were obtained, however, do not follow a pattern of exponential decline (blue; $y = 1.3684e^{-0.02} \times r^2 = 0.1855$).

(D) At 1 year, the percentage of hGPCs in white matter that are Ki67$^+$ (red) exceeds that of the endogenous mouse cells in the same mice (blue), as well as that of untreated rag2 null mice (yellow) and 4-month-old untreated shiverer/rag2 homozygotes (green) in corpus callosum, fimbria, and cerebellum.

1987, 1989), neural stem cells (Mitome et al., 2001; Yandava et al., 1999), and embryonic stem cell-derived glia (Nistor et al., 2005) could give rise to myelinogenic oligodendrocytes in the shiverer mouse, as well as in other animal models of hypomyelination, including the myelin-deficient rat (Archer et al., 1994; Hammang et al., 1997) and shaking pup (Archer et al., 1997). However, none of these efforts yielded sufficiently abundant or extensive myelination to provide significant survival or long-term functional benefit to the treated recipients. In contrast, our present results suggest the feasibility of an outright rescue of the disease phenotype, using highly enriched preparations of human glial progenitor cells delivered to multiple sites of the neonatal neuraxis, at relatively high cell-dose levels.

Only a minority of the transplanted shiverers were rescued by neonatal transplantation. A major challenge going forward will be to better define the critical sites that need to be rapidly myelinated to avoid death, and hence allow progressive myelination to ultimately assuage disease progression. Our results suggest that early myelination of the brainstem, and an early transplant-associated diminution in seizure activity, are both associated with clinical rescue; as such, future studies may combine antiepileptic treatment with more posteriorly biased progenitor grafts, as a potential strategy to improve the likelihood of clinical rescue. These caveats aside, our results indicate that multifocal perinatal transplantation of human glial progenitor cells can be sufficient to rescue a congenital lethal hypomyelination. The sustained viability and restored functional competence of these animals augers well for the potential utility of this approach in the treatment of precociously apparent leukodystrophies, in particular those hypomyelinating disorders manifesting neonatally, such as Pelizaeus-Merzbacher disease (PMD; Garbern and Hobson, 2002; Nave and Griffiths, 2004; Powers, 2004). The pathological similarity of PMD, an X-linked misexpression of proteolipid protein, to the periventricular leukomalacia of cerebral palsy (Deguchi et al., 1997; Rezaie and Dean, 2002; Volpe, 2001), suggests the potential applicability of this glial progenitor cell-based treatment strategy to a wide range of hereditary and ischemic (Back et al., 2001) childhood disorders of myelin.

EXPERIMENTAL PROCEDURES

Cells

Fetal GPCs were extracted from second trimester human fetuses (19–22 weeks gestational age [GA]), obtained at abortion as described (Windrem et al., 2004). The forebrain ventricular/subventricular zones were dissected from the remaining brain parenchyma, the samples chilled on ice, and the minced samples then dissociated using papain/DNase as described (Keyoung et al., 2001), always within 3 hr of extraction. The dissociates were maintained overnight in minimal media of DMEM/F12/N1 with 20 ng/ml FGF. A total of five tissue samples (one at 19 weeks GA, one at 20 weeks, and three at 22 weeks) were used for this study, all from chromosomally normal fetal donors. All samples were obtained with consent under approved protocols of the University of Rochester, Cornell/New York Presbyterian Hospital, and Albert Einstein College of Medicine/Jacobi Hospital Institutional Review Boards.

Sorting

Glial progenitor cells were isolated from dissociated tissue using a dual immunomagnetic sorting strategy. On the day after dissociation, the cells were incubated with mouse anti-PSA-NCAM (Chemicon) at 1:100, then washed and labeled with microbead-tagged rat antimouse IgM (Miltenyi Biotech), and removed by MACS depletion. The remaining PSA-NCAM$^-$ cells were next incubated 1:1 with mAb A2B5 supernatant (clone 105; ATCC, Manassas, VA) for 20 min, then washed and labeled with microbead-tagged rat antimouse IgM (Miltenyi Biotech). All incubations were done on ice (Keyoung et al., 2001; Roy et al., 2000). Magnetic separation of A2B5$^+$ cells (MACS; Miltenyi) was then performed, as described (Nunes et al., 2003). The bound cells were then eluted, yielding a highly enriched population of A2B5$^+$/PSA-NCAM$^-$ cells. After sorting, the cells were maintained in vitro for 1–2 days in DMEM/F12/N1 with 20 ng/ml bFGF, then frozen and stored in liquid nitrogen at 2×10^6 cells/ml in 7% DMSO/93% FBS.

Transplantation and Husbandry

Homozygous shiverers were crossed to homozygous rag2 null immunodeficient mice (Shinkai et al., 1992) to generate a line of shi/shi × rag2$^{-/-}$ myelin-deficient, immunodeficient mice. Newborn pups of this line were transplanted within a day of birth, using a total of 300,000 donor cells dispersed over five injection sites. The pups were first cryoanesthetized for cell delivery, and then 5×10^4 donor cells in 0.5 μl HBSS were injected at each of four locations in the forebrain subcortex, specifically into the anterior and posterior anlagen of the corpus callosum bilaterally. These injections were delivered to a depth of 1.0–1.2 mm ventrally, depending on the weight/size of the pup (which varied from 1 to 1.5 g). A fifth injection of 10^5 cells in 1 μl was delivered into the cerebellar peduncle dorsally, to gain access to the major cerebellar and dorsal brainstem tracts. All cells were injected through pulled glass pipettes, inserted directly through the skull into the presumptive target sites. The pups were then returned to their mother, until weaning at 21 days; at that point, each litter was moved to separate housing. After weaning, mice were checked at least twice daily. Mice that died from immediate surgical complications or before weaning (two saline injected and one GPC transplanted) were excluded from the experiment. Typically as of 130 days of age, mice in all groups began to die. They were checked several times daily, and if found so moribund as to be unable to right themselves upon being moved, they were given barbiturate anesthesia, then perfusion fixed with HBSS followed by 4% paraformaldehyde. When mice were instead found dead, their brains were removed and postfixed for 2 hr in cold paraformaldehyde.

Survival Analysis and Statistics

Kaplan-Meier analysis was used to assess the different survivals of transplanted and control mice, as described (Hosmer and Lemeshow, 1999). No difference in survival was observed between saline-injected and untreated mice, so the two populations were combined as a single control population for the Kaplan-Meier comparison with GPC-implanted mice.

Analyses of variance (ANOVA) were performed using GraphPad Prism (v4.0c for Macintosh; GraphPad Software, San Diego, CA).

Immunolabeling

Human cells were identified with mouse antihuman nuclei, clone 235-1 at 1:100 (MAB1281, Millipore, Billerica, MA). Myelin basic protein was labeled with rat anti-MBP at 1:25 (Ab7349, Abcam, Cambridge, MA), and axons with mouse antineurofilament cocktail at 1:1000 (SMI-311 and SMI-312, Covance, Princeton, NJ). Monoclonal antibodies against Caspr, Nav1.6, and Kv1.2 were used at 1:600, 1:200, and 1:200, respectively, and were obtained from NeuroMab (Davis, CA). Rabbit anti-Caspr and anti-βIV spectrin were generated as described (Rasband and Trimmer, 2001; Yang et al., 2007); rabbit anti-Caspr2

(E and F) Progressive myelination (MBP, green) of mouse axons (neurofilament, in red) was attended by chimerization of the recipient white matter, such that by 20 weeks, host cells (DAPI, blue) are exceeded by human donor cells (human nuclear antigen, hNA, purple, as blue colabeled with hNA, red). (E) Parasagittal section, including dorsal callosum and overlying cortex of a transplanted shiverer at 20 weeks, showing human donor-derived myelination of callosum and admixture of host (blue, DAPI) and donor cells (purple, as blue colabeled with hNA, red). Both myelinated (MBP, green) and unmyelinated (NF, far red) fibers are evident traversing lower cortical layers. (F). Higher magnification section through fimbria of hippocampus, showing myelinated fibers viewed en face, with admixed mouse (blue) and human (purple, representing blue colabeled with hNA, red) cells. Scale bars: 100 μm in (E) and 50 μm in (F).

was obtained from Millipore. Rabbit anti-olig2 was obtained from Abcam (Ab33427) and used at 1:1500. Alexa Fluor secondary antibodies, goat anti-mouse, rat, and rabbit 488, 568, 594, and 647 were used at 1:400 (Invitrogen, Carlsbad, CA).

Myelinated Axon Counts

Uniform random sagittal sections of the cervical spinal cord and coronal sections of the corpus callosum were selected for neurofilament and MBP staining; in the spinal cord samples, the most medial sections were analyzed with respect to the percentage of myelinated host axons. A 1 μm stack of 10 superimposed optical slices taken at 0.1 μm intervals (Olympus FluoView 300) was made for each of three fields of view in the dorsal columns, beginning rostrally and progressing caudally. Three parallel, equidistant lines were laid over the images perpendicular to the axons. Axons were scored at intersections with the lines as either myelinated (closely apposed to MBP on both sides) or unmyelinated. This procedure was then repeated for the coronally cut samples of corpus callosum.

Proportionate Representation of Donor Cells

The percentage of human cells in the recipient white matter was assessed as a function of time after transplantation. Randomly initiated, uniformly sampled sagittal sections of the brains were labeled for human nuclei and DAPI (Vector Labs). Four to six sections (depending on the persistence of the structure in the selected range of sections) of the corpus callosum, fimbria, and cerebellar white matter were counted, with data entry and reconstruction using Bio-Quant. All human nuclei and DAPI-labeled cells in the white matter regions of these 14 μm sections were counted.

Electron Microscopy

The four mice that survived over a year were perfused transcardially with HBSS, followed by 4% paraformaldehyde with 0.25% glutaraldehyde and 6% sucrose in phosphate buffer (sucrose PB). One hemisphere of each brain and longitudinal half of each spinal cord were postfixed in 2% paraformaldehyde, 2.5% glutaraldehyde in sucrose PB for electron microscopy; the other half of each brain and spinal cord were postfixed in 4% paraformaldehyde in sucrose PB for immunohistochemistry. Tissue samples used for electron microscopy were osmicated, dehydrated in ethanol, and embedded in Epon. Ultrathin sectioning was performed using a PowerTome X Ultramicrotome (RMC products by Boeckeler, Tucson, AZ). The ultrathin sections were collected on formvar-coated copper one-hole grids and contrasted with lead citrate and uranyl acetate, then examined in a JEOL 100CX transmission electron microscope.

Seizure Counts

Mice were placed in a sterilized Plexiglas cage with a camera embedded in the ceiling (PhenoTyper, Noldus, Wageningen, The Netherlands) and left undisturbed overnight while their movements were recorded by infrared light. Six nonoverlapping half-hour video segments were randomly selected from each 6 hr videotape, excluding the first 3 hr segment so as to diminish any effects of the novel environment. Two segments for each mouse scored were assigned to each of three observers, blinded as to the mouse's age and treatment. The observers recorded and timed each mouse's seizures, which were defined as such when the mouse fell to its side and assumed a rigid, stereotypically tonic posture, typically complicated by clonic flexion-extension of the trunk and limbs. A seizure was timed as ending when the mouse first moved to right itself. The number of seizures per hour, and the total ictal time per hour, were thereby scored.

Transcallosal Transmission

Mice were anesthetized with ketamine (60 mg/kg, i.p.) and xylazine (10 mg/kg, i.p.), intubated through a tracheotomy, and ventilated with a ventilator (SAR-830, CWE, Inc., Ardmore, PA). A femoral artery was catheterized for monitoring mean artery blood pressure and blood gases, and body temperature was maintained at 37°C by a warming blanket (Harvard Apparatus, Holliston, MA). Mice were secured with a custom-made metal frame that was glued to the skull with acrylic cement. Two burr holes, each 3 mm in diameter, were made bilaterally, centered 1–2 mm posterior to bregma and 2–3 mm from the midline. The dura was removed and agarose (0.75% in saline) was poured into the craniotomy sites, which were then closed with a 0.17 mm-thick glass coverslip. The head frame was then attached to a second frame that was coupled to the microscope stage. Glass micropipettes filled with 2M NaCl solution were then inserted to a depth of 200 μm into the right cortex, at 1.5 mm posterior to bregma and 2.5 mm from the midline, for recording the local field potentials (LFPs) generated by transcallosal electric stimulation. Electrical stimulation (100 μs at 10–1000 μA, via an ISO-Flex isolator controlled by a Master-8 programmer; AMPI, Israel) was applied using a bipolar electrode inserted at the same coordinates in the contralateral (left) hemisphere. Evoked LFPs were recorded by a MultiClamp 700A amplifier, filtered at a cutoff frequency of 1 kHz, and sampled at an interval of 200 μs by a pCLAMP 9.2 program and DigiData 1332A interface (Axon Instruments, Inc.). The same electrode was used to continuously monitor the electrocorticogram (ECoG). ECoG was recorded continuously by a MultiClamp 700A amplifier (Axon) with a low-frequency filter at 1 Hz and high-frequency filter at 100 Hz (51, 52), and a pCLAMP 9.2 program and DigiData 1332A interface (Axon) with an interval of 200 μs. The amplitude of stimulus-evoked transcallosal response was then calculated as the difference between the peak and baseline, whereby the baseline was defined as the average potential measured during the 20 ms before the stimulation was delivered. The velocity of transcallosal response was calculated, together with the latency of the response and the distance between the stimulating and recording electrodes. The response latency was defined as the difference between the stimulus start and the peak. Two recordings of the transcallosal responses to electric stimulation (0.10 ms, 0.01–0.10 mA) were obtained from each animal.

SUPPLEMENTAL DATA

Supplemental Data include two figures and three movies and can be found with this article online at http://www.cellstemcell.com/cgi/content/full/2/6/553/DC1/.

ACKNOWLEDGMENTS

This work was supported by the Miriam and Sheldon Adelson Medical Research Foundation, the G. Harold and Leila Y. Mathers Charitable Foundation, the CNS Foundation and Ataxia-Telangiectasia Children's Project, the National Multiple Sclerosis Society, and NINDS R01NS039559. We thank Devin Chandler-Militello for advice and assistance in cell preparation, and Carolyn Moyle for technical assistance. We are grateful to Brad Poulis of the Fetal Human Tissue Repository of the Albert Einstein College of Medicine for some of the fetal tissue samples used in this study. S.A.G. is a cofounder and shareholder in Q Therapeutics (Salt Lake City, UT), which has licensed relevant patents from the Cornell Research Foundation.

Received: January 2, 2008
Revised: March 5, 2008
Accepted: March 26, 2008
Published: June 4, 2008

REFERENCES

Archer, D., Cuddon, P., Lipsitz, D., and Duncan, I. (1997). Myelination of the canine central nervous system by glial cell transplantation: A model for repair of human myelin disease. Nat. Med. *3*, 54–59.

Archer, D.R., Leven, S., and Duncan, I.D. (1994). Myelination by cryopreserved xenografts and allografts in the myelin-deficient rat. Exp. Neurol. *125*, 268–277.

Back, S.A., Luo, N.L., Borenstein, N.S., Levine, J.M., Volpe, J.J., and Kinney, H.C. (2001). Late oligodendrocyte progenitors coincide with the developmental window of vulnerability for human perinatal white matter injury. J. Neurosci. *21*, 1302–1312.

Deguchi, K., Oguchi, K., and Takashima, S. (1997). Characteristic neuropathology of leukomalacia in extremely low birth weight infants. Pediatr. Neurol. *16*, 296–300.

Eftekharpour, E., Karimi-Abdolrezaee, S., Wang, J., El Beheiry, H., Morshead, C., and Fehlings, M. (2007). Myelination of congenitally dysmyelinated spinal

cord axons by adult neural precursor cells results in formation of nodes of Ranvier and improved axonal conduction. J. Neurosci. *27*, 3416–3428.

Garbern, J., and Hobson, G. (2002). Prenatal diagnosis of Pelizaeus-Merzbacher disease. Prenat. Diagn. *22*, 1033–1035.

Goldman, S. (2005). Stem and progenitor cell-based therapy of the human central nervous sytem. Nat. Biotechnol. *23*, 862–871.

Gumpel, M., Lachapelle, F., Gansmuller, A., Baulac, M., Baron van Evercooren, A., and Baumann, N. (1987). Transplantation of human embryonic oligodendrocytes into shiverer brain. Ann. N Y Acad. Sci. *495*, 71–85.

Gumpel, M., Gout, O., Lubetzki, C., Gansmuller, A., and Baumann, N. (1989). Myelination and remyelination in the central nervous system by transplanted oligodendrocytes using the shiverer model. Discussion on the remyelinating cell population in adult mammals. Dev. Neurosci. *11*, 132–139.

Hammang, J.P., Archer, D.R., and Duncan, I.D. (1997). Myelination following transplantation of EGF-responsive neural stem cells into a myelin-deficient environment. Exp. Neurol. *147*, 84–95.

Hosmer, D., and Lemeshow, S. (1999). Applied Survival Analysis (New York: John Wiley & Sons).

Keyoung, H.M., and Goldman, S.A. (2007). Glial progenitor-based repair of demyelinating neurological diseases. Neurosurg. Clin. N. Am. *18*, 93–104.

Keyoung, H.M., Roy, N., Louissant, A., Benraiss, A., Mori, Y., Okano, H., and Goldman, S.A. (2001). Specific identification, selection and extraction of neural stem cells from the fetal human brain. Nat. Biotechnol. *19*, 843–850.

Lachapelle, F., Gumpel, M., Baulac, C., Jacque, C., Duc, P., and Baumann, N. (1983). Transplantation of CNS fragments into the brains of shiverer mutant mice: Extensive myelination by transplanted oligodendrocytes. Dev. Neurosci. *6*, 325–334.

Learish, R.D., Brustle, O., Zhang, S.C., and Duncan, I.D. (1999). Intraventricular transplantation of oligodendrocyte progenitors into a fetal myelin mutant results in widespread formation of myelin. Ann. Neurol. *46*, 716–722.

Lee, J.P., Jeyakumar, M., Gonzalez, R., Takahashi, H., Lee, P., Baek, R.C., Clark, D., Rose, H., Fu, G., and Clarke, J. (2007). Stem cells act through multiple mechanisms to benefit mice with neurodegenerative metabolic disease. Nat. Med. *13*, 439–447.

Mitome, M., Low, H.P., van Den Pol, A., Nunnari, J.J., Wolf, M.K., Billings-Gagliardi, S., and Schwartz, W.J. (2001). Towards the reconstruction of central nervous system white matter using neural precursor cells. Brain *124*, 2147–2161.

Nave, K.A., and Griffiths, I.R. (2004). Models of Pelizaeus-Merzbacher disease. In Myelin Biology and Disorders, R.A. Lazzarini, ed. (San Diego: Elsevier Academic Press), pp. 1125–1143.

Nistor, G.I., Totoiu, M.O., Haque, N., Carpenter, M.K., and Keirstead, H.S. (2005). Human embryonic stem cells differentiate into oligodendrocytes in high purity and myelinate after spinal cord transplantation. Glia *49*, 385–396.

Nunes, M.C., Roy, N.S., Keyoung, H.M., Goodman, R.R., McKhann, G., Jiang, L., Kang, J., Nedergaard, M., and Goldman, S.A. (2003). Identification and isolation of multipotential neural progenitor cells from the subcortical white matter of the adult human brain. Nat. Med. *9*, 439–447.

Pellegatta, S., Tunici, P., Poliani, P., Dolcetta, D., Cajola, L., Colombelli, C., Ciusani, E., DiDonato, S., and Finocchiaro, G. (2006). The therapeutic potential of neural stem/progenitor cells in murine globoid cell leukodystrophy is conditioned by macrophage/microglial activation. Neurobiol. Dis. *21*, 314–323.

Popko, B., Puckett, C., Lai, E., Shine, H.D., Readhead, C., Takahashi, N., Hunt, S.W., III, Sidman, R.L., and Hood, L. (1987). Myelin deficient mice: expression of myelin basic protein and generation of mice with varying levels of myelin. Cell *48*, 713–721.

Powers, J. (2004). The leukodystrophies: overview and classification. In Myelin Biology and Disorders, R.A. Lazzarini, ed. (San Diego: Elsevier Academic Press), pp. 663–690.

Rasband, M.N., and Trimmer, J.S. (2001). Developmental clustering of ion channels at and near the node of Ranvier. Dev. Biol. *236*, 5–16.

Readhead, C., Popko, B., Takahashi, N., Shine, H.D., Saavedra, R.A., Sidman, R.L., and Hood, L. (1987). Expression of a myelin basic protein gene in transgenic shiverer mice: correction of the dysmyelinating phenotype. Cell *48*, 703–712.

Readhead, C., Takasashi, N., Shine, H.D., Saavedra, R., Sidman, R., and Hood, L. (1990). Role of myelin basic protein in the formation of central nervous system myelin. Ann. N Y Acad. Sci. *605*, 280–285.

Rezaie, P., and Dean, A. (2002). Periventricular leukomalacia, inflammation and white matter lesions within the developing nervous system. Neuropathology *22*, 106–132.

Roach, A., Takahashi, N., Pravtcheva, D., Ruddle, F., and Hood, L. (1985). Chromosomal mapping of mouse myelin basic protein gene and structure and transcription of the partially deleted gene in shiverer mutant mice. Cell *42*, 149–155.

Roy, N.S., Wang, S., Jiang, L., Kang, J., Benraiss, A., Harrison-Restelli, C., Fraser, R.A., Couldwell, W.T., Kawaguchi, A., Okano, H., et al. (2000). In vitro neurogenesis by progenitor cells isolated from the adult human hippocampus. Nat. Med. *6*, 271–277.

Schafer, D.P., and Rasband, M.N. (2006). Glial regulation of the axonal membrane at nodes of Ranvier. Curr. Opin. Neurobiol. *16*, 508–514.

Sherman, D.L., and Brophy, P.J. (2005). Mechanisms of axon ensheathment and myelin growth. Nat. Rev. Neurosci. *6*, 683–690.

Shinkai, Y., Rathbun, G., Lam, K., Oltz, E., Stewart, V., Mendelsohn, M., Charron, J., Datta, M., Young, F., and Stall, A. (1992). RAG2-deficient mice lack mature lymphocytes owing to inability to initiate V(D)J rearrangement. Cell *68*, 855–867.

Snyder, E.Y., Taylor, R.M., and Wolfe, J.H. (1995). Neural progenitor cell engraftment corrects lysosomal storage throughout the MPS VII mouse brain. Nature *374*, 367–370.

Volpe, J.J. (2001). Neurobiology of periventricular leukomalacia in the premature infant. Pediatr. Res. *50*, 553–562.

Windrem, M.S., Nunes, M.C., Rashbaum, W.K., Schwartz, T.H., Goodman, R.A., McKhann, G., Roy, N.S., and Goldman, S.A. (2004). Fetal and adult human oligodendrocyte progenitor cell isolates myelinate the congenitally dysmyelinated brain. Nat. Med. *10*, 93–97.

Windrem, M.S., Roy, N.S., Wang, J., Nunes, M., Benraiss, A., Goodman, R., McKhann, G.M., and Goldman, S.A. (2002). Progenitor cells derived from the adult human subcortical white matter disperse and differentiate as oligodendrocytes within demyelinated lesions of the rat brain. J. Neurosci. Res. *69*, 966–975.

Yandava, B.D., Billinghurst, L.L., and Snyder, E.Y. (1999). "Global" cell replacement is feasible via neural stem cell transplantation: evidence from the dysmyelinated shiverer mouse brain. Proc. Natl. Acad. Sci. USA *96*, 7029–7034.

Yang, Y., Ogawa, Y., Hedstrom, K., and Rasband, M. (2007). βIV spectrin is recruited to axon initial segments and nodes of Ranvier by ankyrinG. J. Cell Biol. *176*, 509–519.